



**HAL**  
open science

# Harvesting information to control non-equilibrium states of active matter

Rémi Goerlich, Luís Barbosa Pires, Giovanni Manfredi, Paul-Antoine  
Hervieux, Cyriaque Genet

► **To cite this version:**

Rémi Goerlich, Luís Barbosa Pires, Giovanni Manfredi, Paul-Antoine Hervieux, Cyriaque Genet.  
Harvesting information to control non-equilibrium states of active matter. 2022. hal-03564197

**HAL Id: hal-03564197**

**<https://hal.science/hal-03564197>**

Preprint submitted on 10 Feb 2022

**HAL** is a multi-disciplinary open access archive for the deposit and dissemination of scientific research documents, whether they are published or not. The documents may come from teaching and research institutions in France or abroad, or from public or private research centers.

L'archive ouverte pluridisciplinaire **HAL**, est destinée au dépôt et à la diffusion de documents scientifiques de niveau recherche, publiés ou non, émanant des établissements d'enseignement et de recherche français ou étrangers, des laboratoires publics ou privés.

# Harvesting information to control non-equilibrium states of active matter

Rémi Goerlich,<sup>1,2</sup> Luís Barbosa Pires,<sup>2</sup> Giovanni Manfredi,<sup>1,\*</sup> Paul-Antoine Hervieux,<sup>1</sup> and Cyriaque Genet<sup>2,†</sup>

<sup>1</sup>Université de Strasbourg, CNRS, Institut de Physique et Chimie des Matériaux de Strasbourg, UMR 7504, F-67000 Strasbourg, France

<sup>2</sup>Université de Strasbourg, CNRS, Institut de Science et d'Ingénierie Supramoléculaires, UMR 7006, F-67000 Strasbourg, France

(Dated: December 22, 2021)

We propose to use a correlated noise bath to drive an optically trapped Brownian particle that mimics active biological matter. Thanks to the flexibility and precision of our setup, we are able to control the different parameters that drive the stochastic motion of the particle with unprecedented accuracy, thus reaching strongly correlated regimes that are not easily accessible with real active matter. In particular, by using the correlation time (i.e., the “color”) of the noise as a control parameter, we can trigger transitions between two non-equilibrium steady states with no expended work, but only a calorific cost. Remarkably, the measured heat production is directly proportional to the spectral entropy of the correlated noise, in a fashion that is reminiscent of Landauer’s principle. Our procedure can be viewed as a method for harvesting information from the active fluctuations.

*Introduction* — Chemical and biological non-equilibrium processes reveal the special role played by fluctuations at mesoscopic scales, raising fascinating questions that form a major topic of current transdisciplinary research [1–3]. The combined development of stochastic thermodynamics and optical trapping experiments offers an appropriate framework to describe such processes with the required focus put on fluctuations [4, 5]. Recently, active fluctuations have been artificially injected inside optical traps by adding correlated (i.e. colored) noises to the trapping potential [6–8]. The engineering of the noise inside the trap offers a new playground where, for instance, optomechanical models of active matter can be studied in close relation with theory [9–12].

In this Letter, we follow this approach to decipher the energetics engaged between non-equilibrium states and correlated baths [13, 14]. To do so, we bring an optically confined microparticle in an active-matter-like non-equilibrium steady state (NESS). The injected correlated noise yields the constant external source of heat needed to maintain, through its consumption, the particle in a chosen NESS. We monitor the non-Brownian diffusion of the trapped bead, and probe large deviations from thermal equilibrium, which correspond to strongly correlated regimes unexplored so far to our knowledge and not accessible with experiments that use real, biological active matter [15–17].

We further demonstrate that it is possible to drive the bead from one NESS to another through the sole change of the correlation time (i.e., the “color”) of the active fluctuations. For instance, transitions between NESS are known to occur when biological matter undergoes a change in mechanical properties, such as during mitosis, and thereby a modification of the intracellular noise spectrum [18, 19]. Modulating the color of the noise without changing its amplitude makes it possible to achieve heat production at constant energy input. We show that this capacity to induce NESS-to-NESS transitions at zero energetic cost is rooted in the informational content of active fluctuations. Indeed, correlated noise carries information that can be quantified by the spectral entropy  $H_s$  [20], the counterpart of Shannon’s entropy in the frequency domain, which

depends on the noise correlation time. Remarkably, we find that, for a constant noise amplitude quantified by an effective temperature  $T_{eff}$ , the heat  $\Delta Q$  generated through the transition is proportional to the entropy of the correlated noise:  $\Delta Q = k_B T_{eff} \Delta H_s$ , in a fashion that is reminiscent of Landauer’s principle. This relation is tested robust over a wide range of heat production and for different noise amplitudes. Effectively therefore, our protocol harvests information from the colored noise and turns it into heat released to the surrounding fluid throughout the NESS-to-NESS transition. Our result makes explicit the deep connection between information and non-equilibrium thermodynamics, which is central to molecular motors and living systems capable of extracting energy from their fluctuating environments to accelerate their average motion, e.g. [21–23].

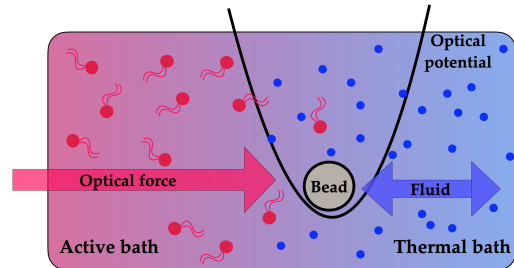


FIG. 1. Schematic view of the experimental realization. The particle is trapped by optical gradient forces using a focused 785 nm laser beam (“optical potential” on the figure). Its stochastic motion is driven by two random baths: a thermal (white noise) bath associated with the surrounding fluid at room temperature  $T = 296$  K (blue) and an active (colored noise) bath generated by an additional 800 nm laser exerting on the bead an actively fluctuating radiation pressure force (red).

*Experimental realization* — Our experiment consists in optically trapping a single 3  $\mu\text{m}$  dielectric bead with a 785 nm Gaussian laser beam. The optical potential created by the gradient forces at the waist of the beam is harmonic, with a stiffness that is proportional to the intensity of the laser. The bead is immersed in water at ambient temperature and undergoes random motion due to the thermal fluctuations consistent with an Ornstein-Uhlenbeck process. An additional radiation pres-

\* giovanni.manfredi@ipcms.unistra.fr

† genet@unistra.fr

sure force is applied to the bead by a second laser, whose intensity is digitally controlled through time by an acousto-optic modulator. Any waveform can be sent on the bead, including noise with arbitrary spectrum, up to  $\approx 10^5$  Hz. A schematic view of the experimental realization is shown in Fig. 1 and the experimental setup is described in Appendix A.

Active particles are characterized by a persistence that can be mimicked by an exponentially correlated Gaussian noise [24–26]. This noise can be generated by an Ornstein-Uhlenbeck process [27, 28]

$$d\eta_t = -\omega_c \eta_t dt + \sqrt{2\alpha\omega_c} dW_t, \quad (1)$$

where  $dW_t$  is a  $\delta$ -correlated Wiener process. Equation (B1) yields a noise  $\eta_t$  with a correlation  $\langle \eta_t \eta_s \rangle = \alpha e^{-|t-s|\omega_c}$ , where  $\omega_c$  is the inverse of the correlation time  $\tau_c$ . The variance of the noise  $\eta_t$  is given by the amplitude factor  $\alpha$  [29]. We emphasize the great flexibility of the above model, which enables us to tune independently the amplitude (variance) and the correlation of the active noise. Thus, we are able to probe a wide range of regimes, from white (small  $\tau_c$ ) to strongly correlated (large  $\tau_c$ ) noises.

The noise  $\eta_t$  is generated numerically using Eq. (B1) and sent to the bead via the radiation pressure of the secondary laser beam –see Appendix B. Hence, the overall motion of the bead is subjected to three forces: the deterministic optical trapping force, the stochastic white noise arising from the thermal bath, and the stochastic colored noise applied by the radiation pressure. The position  $x_t$  of the bead obeys the Langevin equation [16, 24]

$$\dot{x}_t = -\omega_0 x_t + \sqrt{2D}\xi_t + \sqrt{2D_a}\eta_t, \quad (2)$$

where  $\omega_0 = \kappa/\gamma$  is the inverse of the relaxation time in the optical trap, with  $\kappa$  being the stiffness of the trap and  $\gamma$  the Stokes viscous drag. The stochastic variable  $\xi_t$  is a white noise that models the fluid thermal bath, with thermal diffusion coefficient  $D = k_B T/\gamma$ , where  $k_B$  is the Boltzmann constant and  $T$  the temperature of the fluid.  $D_a$  is the *active* diffusivity associated with the colored noise  $\eta_t$ , which incorporates therefore the optomechanical coupling between the bead and the noisy radiation pressure. Note that the model equation (D1) describes a non-Markovian stochastic process that does not respect the fluctuation-dissipation theorem, as the fluctuating force  $\eta_t$  possesses an intrinsic correlation time, whereas the friction term  $\gamma\dot{x}_t$  is instantaneous. Hence, the fluctuations of the active bath are not compensated by the dissipation at the same rate [17], as discussed and probed in detail in Appendix E.

*Out-of-equilibrium properties* — One remarkable feature of active matter is that, due to the correlation properties of the bath, it diffuses in non-Brownian fashion [11, 16, 30, 31]. The appropriate observable to estimate the departure from Brownian motion is the mean square displacement  $\text{MSD}(\Delta) \equiv \langle \delta x^2(\Delta) \rangle = \langle (x_{t+\Delta} - x_t)^2 \rangle$ , where  $\Delta$  is a lag time. In general in the short-time limit, the bead will explore the available space inside the trap according to the free diffusive motion  $\text{MSD} \sim \Delta^\beta$ , with  $\beta = 1$  for normal diffusion and  $\beta \neq 1$  for anomalous diffusion [32, 33].

In Fig. 2 (a), we present the MSD for two processes, obeying Eq. (D1) with the radiation pressure injecting in the trap either a colored noise, or a white noise of equal amplitude. In the latter case, two white noises (thermal and radiation pressure) drive the bead and the data can be fitted with the standard Ornstein-Uhlenbeck MSD  $\langle \delta x^2(\Delta) \rangle = 2D_{eff}(1 - \exp(-\omega_0\Delta))/\omega_0$ . Using the experimental value for the relaxation time  $\omega_0^{-1}$  in the trap, we determine an effective diffusion coefficient  $D_{eff} = 0.29 \mu\text{m}^2/\text{s}$ . The colored noise data is fitted with a modified expression that can be found in [16, 34, 35]. This expression takes into account the noise correlation and where the unique fitting parameter is the active diffusion coefficient  $D_a$  in this way extracted. The superdiffusive nature of the process is clearly visible at short times, with a slope  $\beta = 1.5$ . By tuning the correlation time  $\tau_c$  and the amplitude  $\langle \eta_t^2 \rangle = \alpha$  of the noise  $\eta_t$  injected inside the trap, we can probe different regimes of correlated noise. Of course, all regimes are characterized by a departure from the thermal, white noise equipartition condition  $\langle x_t^2 \rangle = D/\omega_0$ , as a signature of the non-equilibrium nature of the system [16, 25].

When the added colored noise is almost white, i.e. when  $\tau_c \omega_0 \ll 1$ , the bead is driven by two, uncorrelated white noises – see Eq. (D1) – yielding a close-to-equilibrium relation  $\langle x_t^2 \rangle \approx (D + D_a)/\omega_0$  between the motional variance  $\langle x_t^2 \rangle$  and the resulting white noise diffusion coefficients  $D + D_a$  [36]. The variance  $\langle x_t^2 \rangle$  is determined experimentally from the recorded trajectories. Importantly, this case leads to a modified equipartition with an effective temperature  $k_B T_{eff} = \kappa(D + D_a)/\omega_0$  that directly depends on the choice of the active diffusion coefficient  $D_a$  [24, 37]. This weakly correlated regime has been studied both theoretically [11] and experimentally using colloidal beads confined in a bath of swimming *E. coli* bacteria [16].

But our ability to manipulate both the color and the amplitude of the noise leads us to investigate strong deviations from equilibrium in the regime of long correlations times that have not been explored experimentally so far. For such long correlation times  $\tau_c \omega_0 \simeq 1$ , we clearly observe in Fig. 2 (b) that the measured variances depart from the white noise  $D + D_a$  linearity. In this strongly correlated case, the relation between variance and diffusivity can be evaluated from the long-time limit of the MSD with  $\langle \delta x^2(\Delta \gg \tau_c) \rangle = 2\langle x_t^2 \rangle \approx \omega_0^{-1}(D + \alpha D_a/(\omega_0 + \omega_c))$  (see Appendix D). This law fits well the experimental data [red line in Fig. 2 (b)] and the discrepancy between the two blue and red curves quantifies the deviation from equipartition. An important consequence of the explicit dependency of  $\langle x_t^2 \rangle$  on  $\omega_c$  is that one cannot define a unique effective temperature to describe the system both in the short and long time limits [38].

*Transition protocols between two NESS* — The correlation time of the noise may further be used as a control parameter in a protocol that brings the system from one NESS to another, without changing either the confining potential or the temperature. The simplest possible protocol is a step-like sudden change of the correlation time  $\tau_c$  (referred to as “STEP protocol” hereafter), while keeping the noise amplitude constant. We apply the STEP protocol on the system at a low repetition

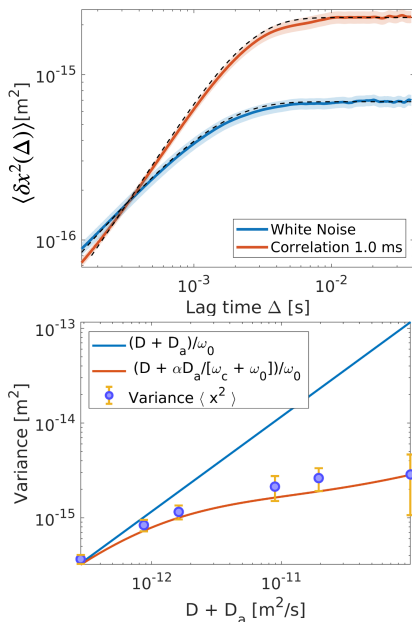


FIG. 2. (a) Mean square displacement measured experimentally for a white noise added to the existing thermal fluctuations inside the fluid (blue line), showing a short-time diffusive limit ( $\sim \Delta^{0.94}$ ), and a correlated noise with  $\tau_c = 1$  ms (red line), yielding a short-time superdiffusive limit ( $\sim \Delta^{1.5}$ ); the superimposed dashed lines are the MSD expected from theory, with a Ornstein-Uhlenbeck MSD evaluated for the white noise case (taking  $T = 296$  K,  $\omega_0^{-1} = 1.2$  ms and extracting a thermal diffusion coefficient  $D_{eff} = 0.29 \mu\text{m}^2/\text{s}$ ) and a modified MSD in the correlated-noise case detailed in Appendix D. The best fit yields an active diffusion coefficient  $D_a = 1.44 \mu\text{m}^2/\text{s}$ , to be compared with the thermal diffusion coefficient  $D$ . The shaded regions accounts for the uncertainties associated with the fitting error in determining  $\omega_0$  and the systematic error in the sphere radius determination. (b) The relation between motional variance  $\langle x_t^2 \rangle$  and the  $D + D_a$  diffusivity is measured on a 99.7% confidence level (blue dots and 3- $\sigma$  bars) for different correlation times ranging from  $\tau_c = 0.1$  ms to  $\tau_c = 100$  ms, with relaxation time inside the optical trap  $\omega_0^{-1} = \gamma/\kappa \approx 1.2$  ms. A naive equipartition result (straight blue line) that would assimilate the correlated noise to a white noise of same amplitude clearly departs from the experimental results, except for very short correlation times. The correct variance estimation for the correlated noise is given by the red curve drawn by taking the  $D_a$  value extracted from the correlated noise MSD. It fits well the experimental data (see Appendix D for further details).

rate, so that it reaches a steady state in between each change of  $\tau_c$ . The ergodic hypothesis, carefully verified (see Appendix C), leads us to build an ensemble of  $\approx 1.1 \times 10^4$  independent trajectories experiencing the same protocol. The main quantity of interest here will be the variance of the response of the bead  $\langle x_t^2 \rangle$  [39].

In Fig. 3, we show the results of a STEP protocol where the correlation time is suddenly changed from  $\tau_c = 0.8$  ms to  $\tau_c = 40$  ms, while  $\omega_0^{-1} = 2.1$  ms. A number of realizations of the noise variable  $\eta_t$  are displayed in Fig. 3 (a): the change in correlation time at  $t = 0$  is clearly visible. In Fig. 3 (b), we represent the variance of the positions of the bead, which undergoes a threefold increase when the correlation time is

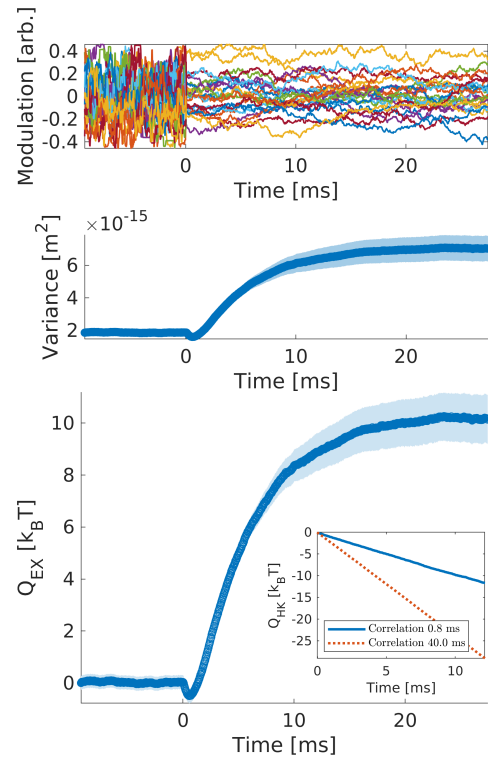


FIG. 3. STEP protocol using the noise correlation time as control parameter. (a) Several digital realizations of the noise variable  $\eta_t$ , undergoing a change in the correlation time at  $t = 0$ , from  $\tau_c = 0.8$  ms before the STEP to  $\tau_c = 40$  ms after. (b) Corresponding experimental ensemble variance  $\langle x_t^2 \rangle$  of the positions of the bead; the shaded area represents the 99.7% confidence interval. (c) Main plot: Cumulative excess heat in units of  $k_B T$ . Inset: Cumulative housekeeping heat before the STEP (blue line) and after the STEP (red dotted line). In the inset, the time origin was reset so as to correspond to the beginning of the steady state for each regime. Sign conventions for the heat terms are used in agreement with [40].

changed. The small dip right after the STEP is due to the fact that the non-Markovian trajectory  $x_t$  is an integral of the noise  $\eta_t$ , hence needs a finite time to probe the total amplitude of  $\eta_t$ .

The above STEP protocol has the same effect (increase in the variance  $\langle x_t^2 \rangle$ ) as a protocol where the noise remains white, but its amplitude (temperature) increases [41–43]. The important difference is that, in our case, we do not change the amplitude of the noise, but only act on its spectrum by modifying the correlation time. In this sense, the protocol can seem costless from the experimentalist’s point of view, as no additional power has to be provided to the laser source at the transition time. As a comparison, we estimated the equivalent power needed to induce the same increase in variance as in Fig. 3 (b) through a change in the noise amplitude, i.e., by changing the diffusivity  $D_a$ . The result is that one would need a laser intensity of 70 mW, whereas we used only 36 mW in our color-based protocol.

From a thermodynamic point of view, our color-based protocol necessarily produces heat, which is then released in the thermal bath. Following Sekimoto’s treatment [40, 44], which was recently applied to active matter [13], the cumulative

stochastic heat can be written as (see Appendix F):

$$q(t) = \frac{1}{2} \int_0^t \kappa \frac{dx^2}{dt'} - \gamma \int_0^t \sqrt{2D_a} \eta_{t'} \dot{x}_{t'} dt'. \quad (3)$$

The first term accounts for the *excess* heat released during a transient evolution of the distribution, and vanishes for steady states [45]. The second term, expressed in terms of the cross-correlation  $\langle \eta \dot{x} \rangle$ , can be evaluated analytically by injecting  $\dot{x}$  as from Eq. (D1) and is shown to grow linearly in time at steady state (see Appendix F). This is the *housekeeping* heat, representing the constant expense needed to maintain the system in its NESS.

Both heat terms are shown in Fig. 15(c). The main graph represents the excess heat dissipated during the transient, with an energy release of  $\approx 10k_B T$ . In the inset, we display the housekeeping heat during the steady states, both before and after the protocol, showing that changing the correlation time affects the heat dissipation rate. Interestingly, the powers at play  $dQ_{HK}/dt \sim 2k_B T/\text{ms}$  in our optical trapping experiments are close to those involved in biological processes such as axonal transport, where kinesin consumes around  $[0.4 - 0.8] k_B T/\text{ms}$  [46–48].

*Harvesting information from the noise* — The protocol described in the above paragraphs seems to raise a paradox: after the transition, the heat released during the process appears to increase (see Fig. 15), while no further energy was injected in the system since only the spectrum of the noise was changed and not its amplitude. As the first principle of thermodynamics is of course not violated, this means that the coupling between the correlated noise bath and the bead has increased, so that energy can be transferred more efficiently from the former to the latter. Such a modulation of the coupling is exactly what happens when the correlation time of the active fluctuations is modified.

Nevertheless, it is illuminating to analyze this situation from an informational point of view. Indeed, a correlated noise carries more information and has lower entropy than a white, or a less correlated, noise. This information content can be measured by the spectral entropy  $H_s$ , which is just the Shannon entropy in the frequency domain [20]:

$$H_s = -k_B \sum_{i=1}^N P(\omega_i) \ln P(\omega_i), \quad (4)$$

where  $P(\omega_i) = S_\eta(\omega_i) / \sum_i S_\eta(\omega_i)$ , and  $S_\eta(\omega_i)$  denotes the power spectral density of the signal  $\eta$  at frequency  $\omega_i$ . The spectral entropy vanishes for a monochromatic signal and reaches its maximum  $k_B \ln N$  for white noise. Any correlated noise has an intermediate value of  $H_s$ , which can be used to measure its information content.

We measured  $H_s$  for various correlation times, but also several noise amplitudes. Each amplitude is labeled by an effective temperatures  $T_{eff}$ , determined by sending a white noise of same amplitude as each colored noise cases. The spectral entropy  $H_s$  is then compared to the generated excess heat. More precisely, for each effective temperature, we define  $\Delta H_s = H_s(\tau_c) - H_s(\tau_{ref})$ , and similarly for  $\Delta Q_{ex}$ , where  $\tau_{ref} = 0.5$  ms is taken as a reference correlation time.

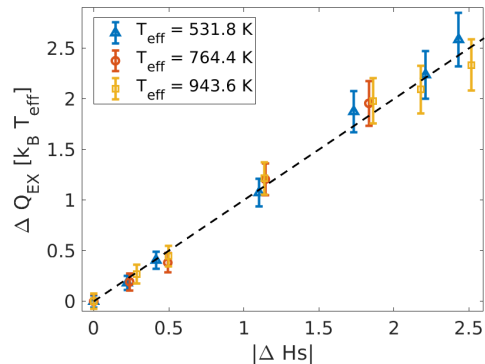


FIG. 4. Measured excess heat between two NESS (in units of  $k_B T_{eff}$ ) plotted as a function of the calculated spectral entropy, for three values of the noise amplitude, each characterized by an effective temperature  $T_{eff}$ —experimental details given in Appendix G. The dashed line has a slope equal to unity.

Hence,  $\Delta H_s$  and  $\Delta Q_{ex}$  represent respectively the informational expenditure and the corresponding energetic cost to go from the reference case to the colored case with correlation time  $\tau_c$  through the STEP protocol described above.

The data from several measurements are plotted in Fig. 4 and obey very neatly the relation  $\Delta Q_{ex}/k_B T_{eff} = \Delta H_s$ . This is a striking proof that the excess heat produced in the process corresponds exactly, in units of  $k_B T_{eff}$ , to the injected information. Note that this expression is highly non-trivial: the left-hand side is a thermodynamic quantity related to the diffusive motion of the trapped bead, while the right-hand side captures the informational content of the colored bath generated by the laser beam. This expression is fully in line with Landauer’s principle [49, 50] where the physical nature of information is seen in the context of active matter. This remarkable result highlights the informational nature of our process, resolving what could appear as a paradoxically costless protocol.

*Conclusion* — In this work, we studied experimentally the diffusive motion of an optically trapped particle subjected to both a white thermal noise due to the surrounding fluid and a correlated noise generated by a digitally controlled fluctuating radiation pressure. This configuration constitutes a very accurate, controllable model of active biological matter.

Three major results were obtained: (i) thanks to the flexibility of our setup, we could explore an unprecedented range of regimes, most notably those characterized by long correlation times and strong amplitudes, which are unattainable in experiments with real active matter; (ii) by using the correlation time as a control parameter, we devised a protocol that drives the system from one non-equilibrium steady state to another, at zero nominal energetic cost; (iii) finally, we showed that the excess heat released during such a protocol is proportional to the spectral entropy of the colored noise, a relationship that is akin to Landauer’s principle of equivalence between information and energy cost [51, 52]. Effectively, the protocol harvests information from the colored noise, turns it into heat necessary for the transition between the two non-

equilibrium states, and finally releases it to the surrounding environment. The ubiquity of non-equilibrium steady states in biological systems, including changes in the spectrum of the bath through time (for example during mitosis [18, 19]) suggests exciting applications for the present findings.

### ACKNOWLEDGMENTS

We thank Samuel Albert, Minghao Li, and Laurent Mertz for discussions. This work of the Interdisciplinary Thematic Institute QMat, as part of the ITI 2021 2028 program of the University of Strasbourg, CNRS and Inserm, was supported by IdEx Unistra (ANR-10-IDEX- 0002) and by SFRI STRATUS project (ANR-20-SFRI-0012), and by ANR Equipex Union (ANR-10-EQPX-52-01), the Labex NIE projects ANR-11-LABX-0058-NIE, and USIAS (ANR-10-IDEX- 0002-02) under the framework of the French Investments for the Future Program.

### Appendix A: Experimental setup and calibration

Our experimental setup consists in optically trapping, in a harmonic potential, a single dielectric bead ( $3\ \mu\text{m}$  polystyrene sphere) in a fluidic cell filled with dionized water at room temperature. The harmonic potential is induced by focusing inside the cell a linearly polarized Gaussian beam ( $785\ \text{nm}$ , CW  $110\ \text{mW}$  laser diode, Coherent OBIS) through a high numerical aperture objective (Nikon Plan Apo VC,  $60\times$ ,  $\text{NA}= 1.20$  water immersion, Obj1 on Fig. 5). An additional force in the form of radiation pressure is applied to the sphere using an additional high-power laser ( $800\ \text{nm}$ , CW  $5\ \text{W}$  Ti:Sa laser, Spectra Physics 3900S). The intensity of this radiation pressure beam is controlled by an acousto-optic modulator (Gooch and Housego 3200s, AOM on Fig. 5) using a digital-to-analogue card (NI PXIe 6361) and a PYTHON code.

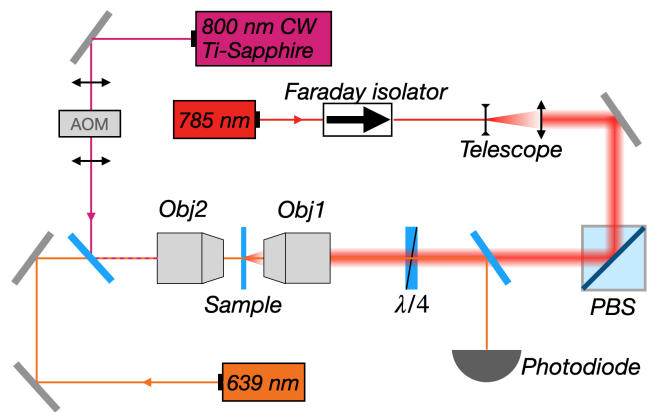


FIG. 5. Simplified view of the optical trapping setup. The sphere is suspended in water inside the *Sample* cell inserted between the two objectives Obj1 and Obj2. The  $785\ \text{nm}$  trapping beam is drawn in red, the  $800\ \text{nm}$  radiation pressure beam in purple. The intensity of this beam controlled by the acousto-optic modulator (AOM). The instantaneous position of the trapped bead is probed using the auxiliary  $639\ \text{nm}$  laser beam, drawn in orange, whose scattered signal is sent to a high-frequency photodiode.

The instantaneous position  $x_t$  of the sphere along the optical axis is measured by recording the light scattered off the sphere of a low-power  $639\ \text{nm}$  laser (CW  $30\ \text{mW}$  laser diode, Thorlabs HL6323MG), sent on the bead via a second objective (Nikon Plan Fluor Extra Large Working Distance,  $60\times$ ,  $\text{NA}= 0.7$ , Obj2 on the figure). The scattered light is collected by Obj1 and recorded by a photodiode ( $100\ \text{MHz}$ , Thorlabs Det10A). The recorded signal (in  $\text{V/s}$ ) is amplified using a low noise amplifier (SR560, Stanford Research) and then acquired by an analog-to-digital card (NI PCI-6251). The signal is filtered through a  $0.3\ \text{Hz}$  high-pass filter at  $6\ \text{dB/oct}$  to remove the DC component and through a  $100\ \text{kHz}$  low-pass filter at  $6\ \text{dB/oct}$  to prevent from aliasing. The scattered intensity varies linearly with the position of the trapped bead  $x_t$  for small enough displacements and we make sure to work in the linear response regime of the photodiode so that the recorded signal is linear with the intensity, resulting in a voltage trace well linear with  $x(t)$ .

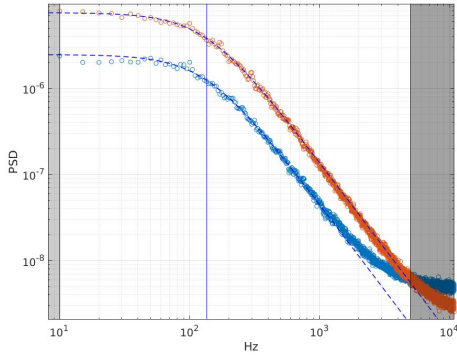


FIG. 6. Power spectral density  $S_x[\omega]$  of the bead position, recorded with no additional noise, i.e. solely driven by thermal fluctuations (blue circles) and with additional white noise injected inside the trap (red circles) using the auxiliary radiation pressure laser made noisy via the AOM. In both cases, the dashed lines correspond to Lorentzian fits, with shaded regions indicate the limits of the fits. The vertical line mark the position of the trap roll-off frequency at  $\sim 10^2$ Hz. Note the onset of the electronic noise floor at high frequencies.

The calibration of the recorded voltage is done by fitting the motional Lorentzian spectrum of the sphere -see Fig. 6- from which is extracted a calibration coefficient expressed in  $\text{m/V}$ , generally  $\sim 10^{-7}\text{m/V}$ . The noise added by the radiation pressure laser modifies the dynamics of the bead, but without changing the properties of the trapping potential. As presented in Fig. 6, we carefully verify that an added white noise that mimics a higher temperature, only leads to an increase in the power spectral density amplitude (as expected when increasing the kinetic temperature of the bead) without modifying neither its Lorentzian profile nor the roll-off frequency of the trap, left unchanged at  $\approx 150\text{Hz}$ .

### Appendix B: External radiation pressure force acting as a bath: from noise generation to active protocols

We generate the external noise following the sequence described in Fig. 7. Using a PYTHON code with a build-in random noise generator, we can easily generate a white noise for which the choice of the distribution function of the noise has no influence on  $x(t)$  (by the virtue of the central limit theorem with all noise events being independent). To maximize the usable dynamical range, we thus simply use a uniformly distributed noise.

In contrast, for a colored noise, both correlation and distribution matter. In this case, we use a Gaussian exponentially correlated noise, given as the solution of the Ornstein-Uhlenbeck process

$$d\eta_t = -\omega_c \eta_t dt + \sqrt{2\alpha\omega_c} dW_t, \quad (\text{B1})$$

where  $\omega_c$  is the inverse characteristic time of the noise and  $\sqrt{\alpha}$  its amplitude. The variance of such a process is  $\langle \eta_t^2 \rangle = \alpha$ .

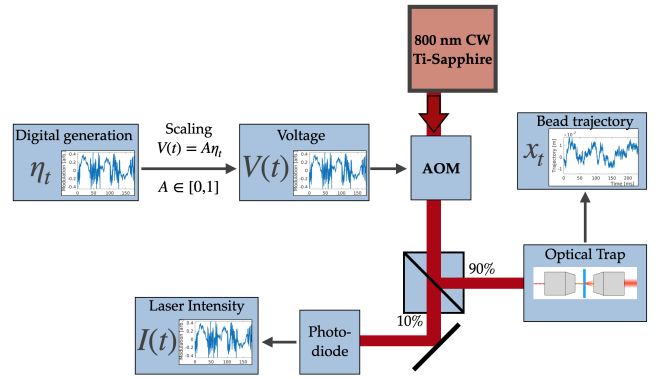


FIG. 7. Schematic representation of the signal and data acquisition processing implemented in our experiments. The noise  $\eta_t$  is digitally generated, scaled to a voltage  $V(t)$  that can be sent to the acousto-optic modulator (AOM), producing a diffracted beam whose intensity varies linearly with this input voltage. The laser beam diffracted through the AOM exerts a radiation pressure on the optically trapped sphere, whose position is recorded as detailed in Sec. A. A small part of the laser beam is also measured and used to monitor and evaluate the noise  $\eta_t$  as it enters the trap.

This correlated noise will then enter into the Langevin equation as an external random force field

$$\gamma \dot{x} = -\kappa x_t + \gamma \sqrt{2D} \xi_t + F_{ext}(t) \quad (\text{B2})$$

with  $D = k_B T / \gamma$  the diffusion coefficient in the thermal bath. The external radiation pressure force  $F_{ext} = F_0 + \delta F(t)$  is centered around a mean value  $\langle F_{ext} \rangle = F_0$  and with a zero mean noise part  $\langle \delta F(t) \rangle = 0$ . The average term  $F_0$  vanishes trivially when looking at the centered process  $x_t - \langle x_t \rangle = x_t - F_0 / \kappa$ , which is always the case in our experiments. Random, the external force acts as a secondary bath. It can thus be recast as  $F_{ext}(t) = \gamma \sqrt{2D_a} \eta_t$ , i.e. on the same footing as the thermal force  $F_{th}(t) = \gamma \sqrt{2D} \xi_t$  where  $D$  is in  $\text{m}^2/\text{s}$  and  $\xi$  (the time derivative of a Wiener process) is in  $\sqrt{\text{Hz}}$ . This leads us to introduce an *active* diffusion coefficient  $D_a$  having the same dimension as  $D$ , associated with the noise  $\eta_t$  solution of Eq. (B1). This gives the noise of dimension  $[\eta_t] \equiv [\sqrt{\alpha}] \equiv \sqrt{\text{Hz}}$ , just like the thermal noise term  $\xi_t$ .

An important asset of our work is the flexibility of our scheme for controlling the color and the amplitude of the noise, which demands to keep  $\omega_c$  and  $\alpha$  independent. To do so, we first generate numerically with the PYTHON code, under a sampling frequency of 20kHz, the noise  $\eta_t$  of variance  $\alpha$ , scaled to the desired amplitude  $\in [0, 1]$  which corresponds, in Volts, to the range fixed by the radio-frequency generator driving the acousto-optic modulator (AOM). The AOM response is calibrated to yield a linear relation between the input voltage and output laser intensity in the first order diffracted beam. The numerically generated noise is thereby encoded into a radiation-pressure laser intensity noise sent to the bead. This noise intensity acting on the bead depends both on the gain of the AOM-diffracted beam and on the choice of the radiation-pressure laser intensity.

In our experiments, the amplitude of the noise is independent of its color, which is different from the choice made in

[16], where  $\alpha$  scales as the square root of the inverse correlation time of the noise. This choice necessarily induces the interplay between both correlation times and amplitudes that we want to avoid. The actual amplitude of the noise experienced by the bead, which depends not only on the radiation-pressure laser intensity but also on the optomechanical coupling between this laser beam and the trapped sphere, will be taken into account in  $F_{ext}$  via the active diffusion coefficient  $D_a$ . This implies that choosing  $\alpha = 1$  is the simplest option. However, we keep the  $\alpha$  term for clarity, as a purely dimensional constant.

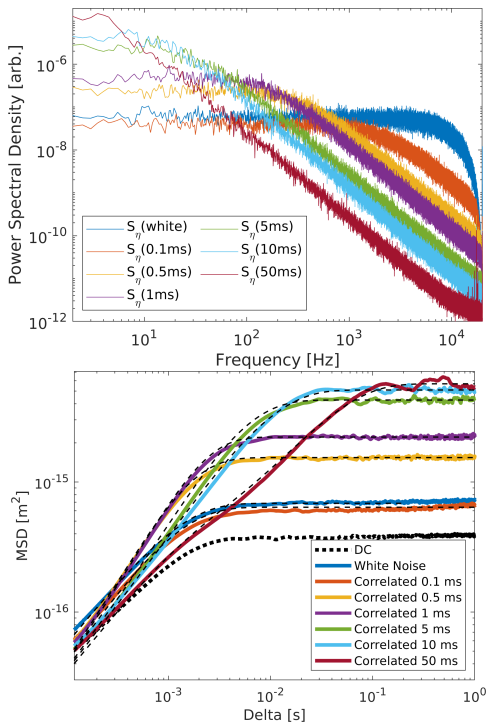


FIG. 8. (a) Power spectral density associated with different noises  $\eta_t$  (for each colored curves, the corresponding correlation time is indicated within brackets in the legend). These spectra are measured directly from the laser intensity signal that is sent on the trapped bead as a radiation pressure. (b) Mean squared displacement of the sphere for each of the noises presented in panel (a). The DC case corresponds to the absence of additional noise, with  $F_{ext} = F_0$ . We observe that the white noise case and the first colored noise case (correlation time 0.1ms) are almost identical. Superimposing the fit performed with the analytical expression for the mean squared displacement (see below, Sec. D) enables one to extract the active diffusion coefficients  $D_a$  for each case.

On Fig. 8 (a), we show the power spectral densities of different noises, from white to colored. At high frequencies ( $> 3000$  Hz, see Fig. 6), the signal is dominated by the electronic noise of the experiment, limiting the spectral bandwidth of interest from a fraction of Hz to a few kHz. The blue curve in Fig. 8 corresponds to a white noise generated over the desired bandwidth where we see its flat spectrum covering all the response region of the bead, up to the 20 kHz limit of the generation sampling frequency. The other curves are the dif-

ferent colored noises, with correlation times spanning from 0.1 to 50 ms. On Fig. 8 (b), we show the mean squared displacement (MSD) associated with each noise. The black curve shows the DC case with  $F_{ext} = F_0$  where no noise is added. The blue curve corresponds to the white noise drive (blue spectrum of Fig. 8 (a)), slightly above the thermal MSD as a consequence of the increase in effective temperature. The orange curve gives the first colored noise case (orange spectrum of Fig. 8 (a)). We can note that the responses to a white noise and to a colored noise of correlation time 0.1 ms are similar, this colored noise being "almost white". This implies that longer ( $> 0.1$  ms) correlation times are needed to make a clear difference between white and colored cases (as seen for the next colored noise with correlation time 0.5 ms). The other curves are the MSD corresponding to the different noises of Fig. 8 (a).

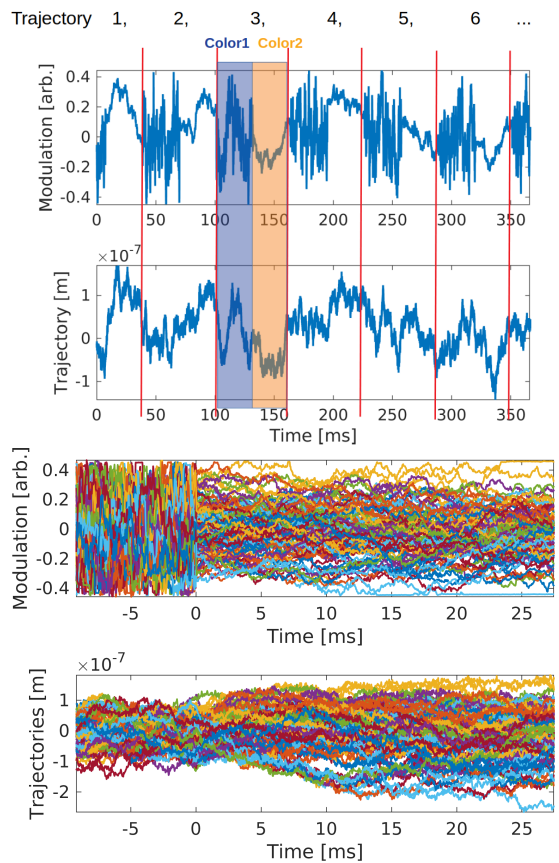


FIG. 9. (a) Temporal noise series  $\eta_t$  modulated between two correlation times (two colors) following a 20 Hz square modulation function (top) and the resulting trajectory  $x_t$  (bottom). (b) Each long trajectory is reshaped as an ensemble. In the upper panel, the  $\{\eta_t^i\}$  ensemble clearly displays at  $t = 0$  the instantaneous change in correlation with constant amplitude. In the lower panel, the ensemble of trajectories  $\{x_t^i\}$  of the bead show the progressive change in the motional variance that results from the step-like change of correlation times of the bath.

To study protocols, we need an ensemble of independent trajectories all experiencing the same parameter changes. In



our experiments, this is a change in correlation time  $\omega_c(t)$  that we modulate in a step-like way from an initial  $\omega_c^i$  to a final  $\omega_c^f$  values. With one single bead in the optical trap, the ensemble is drawn out of a long time series, for which the ergodic hypothesis is crucial and was carefully checked as discussed in Sec. C. We produce one long noise sequence  $\eta_t$  where a large number of correlation time changes are produced following a  $\omega_c^i/\omega_c^f$  square modulation at a low enough repetition rate (a few tens of Hertz). This modulation sequence is sent to the bead via the radiation pressure laser. The corresponding trajectory  $x_t$  of the bead relaxes to one steady-state between each change on  $\omega_c$ . This long trajectory is cut and reshaped into an ensemble of trajectories  $\{x_t^i\}$  that, each, experience a step-like change in correlation time. In order to build the actual noise protocol driving these trajectories, we generate in parallel two independent sequences of  $\eta_t$  time-series with different (but constant) correlation times that are then interspersed synchronously with the  $\omega_c^i/\omega_c^f$  square modulation impacting the motional trajectory  $x_t$ . The detailed procedure is described in Fig. 9.

### Appendix C: Ergodicity

Ergodicity is the equality of time and ensemble averages in the limit of infinite time  $\mathcal{T}$  and infinite ensemble. But as detailed in our previous work [39], appropriate tools exist that can assess the ergodic nature of trajectories  $\{x_t\}$  on finite samples and finite times. To do so, we rely on an estimator [32] corresponding to the variance of the ratio between time averaged mean squared displacement (MSD) and time-ensemble averaged MSD. This ratio should become Dirac-like for long-time (or short time lag  $\Delta$  in the MSD). The 0 limit of the variance of this ratio for  $\Delta/\mathcal{T} \rightarrow 0$  is a necessary and sufficient condition for ergodicity [39].

The result, plotted in Fig. 10 (a) with fixed  $\mathcal{T}$  and varying  $\Delta$ , decays to zero for short time-lag as expected. With fixed  $\Delta$ , varying  $\mathcal{T}$ , the expected decrease towards 0 for long time, with a linear trend in log scale, is also clearly seen in Fig. 10 (b). These two results validate our ergodic assumption for the time-series of position  $x_t$ , and therefore our treatment when it comes to building trajectory ensembles.

### Appendix D: Power spectral density, autocorrelation, mean squared displacement and equipartition breaking

Our system, consisting of an optically trapped bead thermally diffusing within active fluctuations, is described by a couple of stochastic differential equations that determine the evolution of the position of the bead within the trap according to:

$$\dot{x}_t = -\omega_0 x_t + \sqrt{2D}\xi_t + \sqrt{2D_a}\eta_t \quad (\text{D1})$$

where the active noise  $\eta_t$ , solution of the Ornstein-Uhlenbeck process

$$d\eta_t = -\omega_c \eta_t dt + \sqrt{2\alpha\omega_c} dW_t, \quad (\text{D2})$$

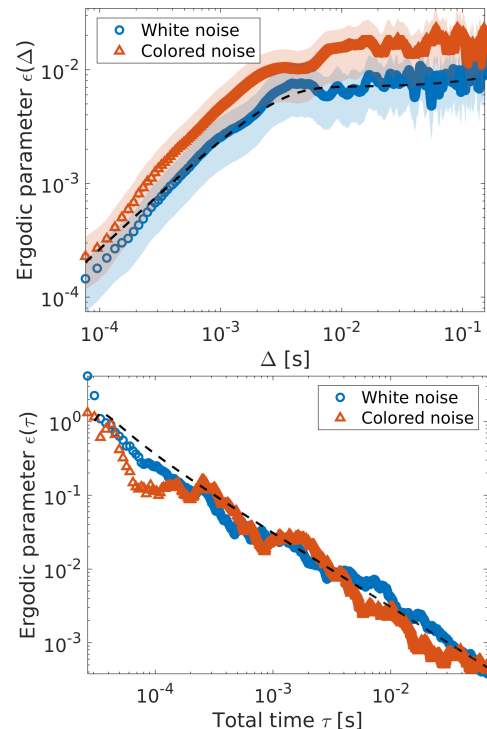


FIG. 10. (a) The ergodic parameter (i.e. the normalized variance  $\epsilon(\Delta)$  presented in our previous work [39]) is shown as a function of the time lag  $\Delta$  for both the white noise driven process (blue circles) and the colored noise driven process (red triangles) along with the analytical prediction for the white noise case (black dashed line). The red and blue hazes measure the 95% confidence interval. (b) The same ergodic parameter  $\epsilon(\Delta)$  plotted as a function of the total time  $\tau$  for both the white-noise driven process (blue circles) and the colored-noise driven process (red triangles) along with the analytical prediction for the white noise case (black dashed line).

is an exponentially correlated Gaussian variable.

We can derive the noise power spectrum density by Fourier transforming Eq. (D2)

$$-i\omega\eta[\omega] = -\omega_c\eta[\omega] + \sqrt{\alpha\omega_c}\xi[\omega] \quad (\text{D3})$$

where  $\omega_c$  is the correlation pulsation. Taking the squared norm leads to the active noise power spectral density (PSD)

$$\eta[\omega]\eta^*[\omega] = |\eta[\omega]|^2 = \frac{\alpha\omega_c}{\omega_c^2 + \omega^2}. \quad (\text{D4})$$

On Fig. 11 (a), we plot the PSD directly measured from the laser output signal used to induce the noisy radiation pressure, both in the case of a white noise and colored noise. As expected, the spectrum of the white noise is flat on all the studied bandwidth, whereas the spectrum of the colored noise is following a Lorentzian profile, well captured by a fit following Eq. (D4).

The PSD of the motion  $x_t$  is evaluated from Eq. (D1) as:

$$x[\omega]x^*[\omega] = \frac{1}{\omega_0^2 + \omega^2} (2D\xi[\omega]\xi^*[\omega] + 2D_a\eta[\omega]\eta^*[\omega]), \quad (\text{D5})$$

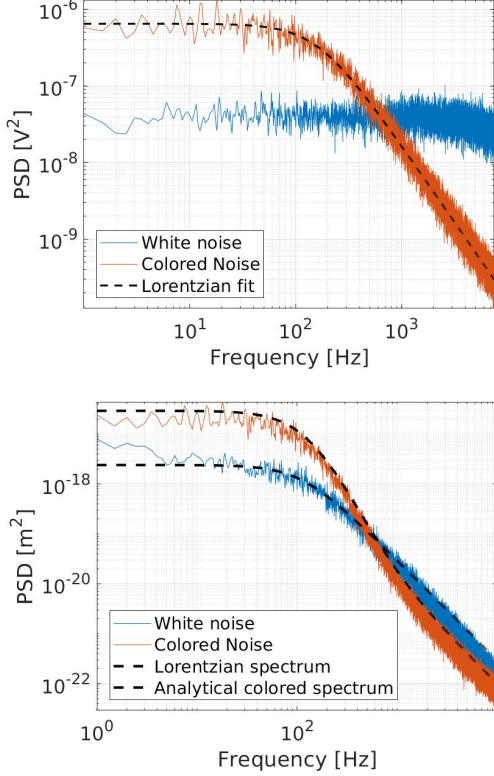


FIG. 11. (a) Power spectral densities (PSD) of the white noise (blue curve) and colored noise (red curve) measured on a 10% fraction of the laser beam signal that is sent inside the trap to act on the bead as a noisy radiation pressure. A Lorentzian fit (black dashed curve) is superimposed on the colored noise spectrum. (b) Motional PSD  $S_x[\omega] = 2|x[\omega]|^2$  plotted as a function of the frequency for the white noise driven process (blue) and the colored noise driven process (red) along with the associated theoretical PSD (black dashed curves).

noting that the implicit averaging performed in this square cancels the two cross-product of the uncorrelated noises  $\eta[\omega]\xi^*[\omega]$  and the complex conjugate. In Eq. (D5),  $\omega_0 = \kappa/\gamma$  is the inverse of the characteristic relaxation time of the system, and  $\eta[\omega]\eta^*[\omega]$  is given by Eq. (D4) and  $\xi[\omega]\xi^*[\omega] = 1$ . Hence

$$x[\omega]x^*[\omega] = |x[\omega]|^2 = \frac{1}{\omega_0^2 + \omega^2} \left( 2D + \frac{2D_a\alpha\omega_c}{\omega_c^2 + \omega^2} \right) \quad (\text{D6})$$

On Fig. 11 (b), we plot the measured spectra of  $x_t$  both for a white and colored external drive, with the analytical result of Eq. (D6) using the value of  $D_a$  obtained from the fit of the MSD for the colored noise (see Fig. 8 above) and using the  $D_a \rightarrow 0$  limit for the white noise case. A very good agreement between the theory and the experimental data is clearly seen, confirming that our model captures well the real diffusive dynamics of the trapped bead.

We can also compute the correlation function of the colored

noise driven process from the Wiener-Khintchine theorem as:

$$\begin{aligned} C_{xx}(\Delta) &= \frac{1}{2\pi} \int_{-\infty}^{+\infty} |x[\omega]|^2 e^{-i\omega\Delta} d\omega \\ &= \frac{1}{2\pi} \int_{-\infty}^{+\infty} \frac{2De^{-i\omega\Delta} d\omega}{\omega_0^2 + \omega^2} \\ &\quad + \frac{1}{2\pi} \int_{-\infty}^{+\infty} \frac{2D_a\alpha\omega_c e^{-i\omega\Delta} d\omega}{(\omega_0^2 + \omega^2)(\omega_c^2 + \omega^2)}, \end{aligned} \quad (\text{D7})$$

where both integrals can be computed via contour integration. For the first one,  $f[\omega] = \frac{D}{\pi} \frac{e^{-i\omega\Delta}}{\omega_0^2 + \omega^2}$  has one simple pole in the upper-half complex plane in  $i\omega_0$ , leading to compute one residue

$$\begin{aligned} \int_{-\infty}^{+\infty} f[\omega] d\omega &= 2i\pi \text{Res}\{f[\omega], i\omega_0\} \\ &= \lim_{\omega \rightarrow i\omega_0} \frac{2De^{-i\omega\Delta}}{\omega + i\omega_0} \\ &= \frac{D}{\omega_0} e^{-\omega_0\Delta}. \end{aligned} \quad (\text{D8})$$

Similarly, the second integral with  $g[\omega] = \frac{D_a\alpha\omega_c e^{-i\omega\Delta}}{\pi(\omega_0^2 + \omega^2)(\omega_c^2 + \omega^2)}$  is evaluated by separating it through partial fraction decomposition in  $g[\omega] = \frac{D_a\alpha\omega_c e^{-i\omega\Delta}}{\pi(\omega_c^2 - \omega_0^2)} \left( \frac{1}{\omega_0^2 + \omega^2} - \frac{1}{\omega_c^2 + \omega^2} \right) \equiv g_1[\omega] + g_2[\omega]$  leading to two integrals with simple poles in  $i\omega_0$  and  $i\omega_c$

$$\begin{aligned} \int_{-\infty}^{+\infty} g[\omega] d\omega &= 2i\pi \text{Res}\{g_1[\omega], i\omega_0\} + 2i\pi \text{Res}\{g_2[\omega], i\omega_c\} \\ &= D_a\alpha\omega_c^2 \left( \frac{e^{-\omega_0\Delta}}{\omega_0(\omega_c^2 - \omega_0^2)} - \frac{e^{-\omega_c\Delta}}{\omega_c(\omega_c^2 - \omega_0^2)} \right) \\ &= \frac{D_a\alpha\omega_c}{\omega_0(\omega_c^2 - \omega_0^2)} \left( e^{-\omega_0\Delta} - \frac{\omega_0}{\omega_c} e^{-\omega_c\Delta} \right). \end{aligned} \quad (\text{D9})$$

These evaluations are combined to provide the expression for the correlation function of the diffusion process:

$$C_{xx}(\Delta) = \frac{D}{\omega_0} e^{-\omega_0\Delta} + \frac{D_a\alpha\omega_c}{\omega_0(\omega_c^2 - \omega_0^2)} \left( e^{-\omega_0\Delta} - \frac{\omega_0}{\omega_c} e^{-\omega_c\Delta} \right) \quad (\text{D10})$$

On Fig. 12 we represent the normalized correlation function  $C_{xx}$  for both white and colored noise drives where we superimpose the analytical result, using the value of  $D_a$  obtained, as indicated above, from the fit of the MSD for the colored noise. Here too, we use the  $D_a \rightarrow 0$  limit for the white noise. Again, the good agreement between the exponential decays and the analytical models is observed.

The MSD of a colloid diffusing in a thermal environment obeys an Ornstein-Uhlenbeck process and is thus characterized by the white noise MSD:

$$\langle \delta x^2(\Delta) \rangle \equiv \langle (x(t+\Delta) - x(t))^2 \rangle = \frac{2D}{\omega_0} (1 - e^{-\omega_0\Delta}) \quad (\text{D11})$$

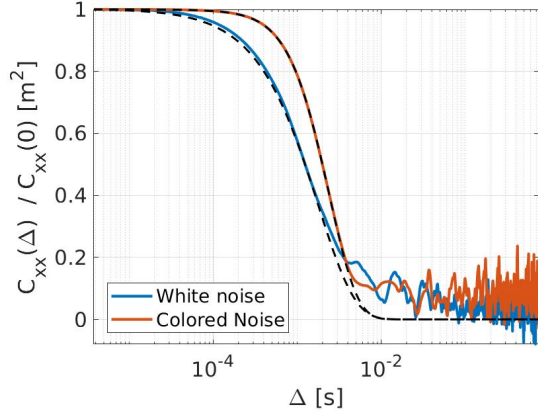


FIG. 12. Correlation function  $C_{xx}(\Delta) = \langle x(t+\Delta)x(t) \rangle$  plotted as a function of the lag  $\Delta$  for the white (blue curve) and colored (red curve) noise-driven processes, both normalized to the zero-delay  $\Delta = 0$  correlation function  $C_{xx}(0)$ . The theoretical expressions derived in Sec. D are displayed as dashed black curves for both cases.

where  $D$  is the diffusion coefficient in the thermal bath, expressed in  $\text{m}^2/\text{s}$ , and  $\omega_0 = \kappa/\gamma$  is the inverse of the characteristic relaxation time of the bead in the trap.

In contrast, the MSD of an active particle obeys Eq. (D1) and can be computed as  $\langle \delta x^2(\Delta) \rangle = 2\langle x_t^2 \rangle - 2C_{xx}(\Delta)$  where the variance is the stationary variance of the process and  $\langle x_t^2 \rangle$  is taken as the limit  $\lim_{t \rightarrow \infty} [\langle x_t^2 \rangle] = \frac{D}{\omega_0} + \frac{D_a \alpha \omega_c}{\omega_0(\omega_c + \omega_0)}$ . This leads us to calculate directly:

$$\begin{aligned} \langle \delta x^2(\Delta) \rangle &= \frac{2D}{\omega_0} + \frac{2D_a \alpha}{\omega_0(\omega_c + \omega_0)} + \frac{2D}{\omega_0} e^{-\omega_0 \Delta} \\ &\quad + \frac{2D_a \alpha \omega_c}{\omega_0(\omega_c^2 - \omega_0^2)} \left( e^{-\omega_0 \Delta} - \frac{\omega_0}{\omega_c} e^{-\omega_c \Delta} \right) \\ &= \frac{2D}{\omega_0} (1 - e^{-\omega_0 \Delta}) \\ &\quad + \frac{2D_a \alpha \omega_c}{\omega_0(\omega_c^2 - \omega_0^2)} \left( 1 - e^{-\omega_0 \Delta} - \frac{\omega_0}{\omega_c} (1 - e^{-\omega_c \Delta}) \right) \end{aligned} \quad (\text{D12})$$

that constitutes the result used in the main text.

The long-time limit can be easily derived as:

$$\lim_{\Delta \rightarrow \infty} [\langle \delta x^2(\Delta) \rangle] = \frac{2D}{\omega_0} + \frac{2D_a \alpha}{\omega_0(\omega_c + \omega_0)}. \quad (\text{D13})$$

To assess the break of the equipartition relation, it is enough to show the absence of linearity between the variance and the effective diffusion coefficient associated with the active process. For different noise colors, we thus measure and fit the MSD to extract each corresponding  $D_a$ . We then plot in Fig. 2, panel (b) of the main text the variance against the total diffusion coefficient  $D + D_a$ . As seen in the figure, we clearly observe that the variance does not follow the intuitive  $\omega_0^{-1}$  linearity. In striking contrast, it rather follows one half of Eq. (D13) – i.e.,  $\frac{D}{\omega_0} + \frac{D_a \alpha}{\omega_0(\omega_c + \omega_0)}$  – where the explicit  $\omega_c$  term prevents us from defining a unique effective diffusion coefficient

(or effective temperature) and where  $D_a$  comes from the fit of the MSD displayed in Fig. 8.

### Appendix E: Micro Rheology and Fluctuation Dissipation Theorem

We probe the non-equilibrium nature of the active fluctuations and the validity of the Fluctuation Dissipation Theorem (FDT) by comparing the dynamical responses of our system to Active MicroRheological (AMR) and Passive MicroRheological (PMR) excitations, respectively [35, 53].

At thermal equilibrium, under detailed balance conditions, the linear response of the system to a small perturbation is connected to equilibrium correlations of fluctuations through the FDT according to which:

$$\frac{\partial C_{xx}(t)}{\partial t} = 2k_B T R(t), \quad (\text{E1})$$

where  $C_{xx}(t) = \langle x(t)x(0) \rangle$  is the motional autocorrelation function and  $R(t)$  is the response function of the system. This equation can be more conveniently derived in the frequency domain. If we consider the motion of the bead driven by a noise of unit variance  $\phi_t$  (that takes in our case the form  $\xi_t + \sqrt{D_a/D}\eta_t$ ), the Fourier transform of the corresponding Langevin equation writes as:

$$-i\omega\gamma x[\omega] = -\kappa x[\omega] + \sqrt{2k_B T}\gamma\phi[\omega], \quad (\text{E2})$$

where  $\kappa$  is the stiffness of the potential,  $\gamma$  the Stokes friction drag, and  $\sqrt{2k_B T}\gamma\phi[\omega]$  is a generic random force. The equation can be written in terms of a mechanical susceptibility  $\chi[\omega]$  as

$$x[\omega] = \chi[\omega] \sqrt{2k_B T}\gamma\phi[\omega] \quad (\text{E3})$$

where  $\chi[\omega]$  can be decomposed into real and imaginary parts as:

$$\chi[\omega] = \frac{\omega_0}{\gamma(\omega_0^2 + \omega^2)} + i \frac{\omega}{\gamma(\omega_0^2 + \omega^2)} \equiv \chi'[\omega] + i\chi''[\omega]. \quad (\text{E4})$$

If we compare the imaginary part  $\chi''[\omega]$  with the power spectral density obtained, in the case of a thermal, white noise drive, by the square modulus of position Fourier transform  $|x[\omega]|^2 = 2D/(\omega_0^2 + \omega^2)$ , we obtain the expression of the FDT in the Fourier space:

$$\chi''[\omega] = \frac{\omega|x[\omega]|^2}{2k_B T} \quad (\text{E5})$$

where the spectrum  $|x[\omega]|^2$  is the Fourier transform of autorrelation function  $C_{xx}(t)$  (Wiener-Khinchine theorem).

If now one adds a small sinusoidal perturbation on the bead by means of an external force (which corresponds to radiation pressure in our experiments), the FDT can be tested experimentally by measuring the response function. Under the sinusoidal  $ac$  drive of the AMR mode at pulsation  $\omega_{ac}$ , the PSD takes the following form [54]

$$|x[\omega]|_{ac}^2 = \frac{1}{\omega_0^2 + \omega^2} \left( 2D + \frac{F_{ac}^2}{2\gamma^2} \delta(\omega - \omega_{ac}) \right) \quad (\text{E6})$$

where  $F_{ac}$  is the Fourier force component of the drive, while the unperturbed PSD of the PMR mode writes

$$|x[\omega]|^2 = \frac{2D}{\omega_0^2 + \omega^2}. \quad (\text{E7})$$

By computing the ratio  $|x[\omega_{ac}]|^2/|x[\omega_{ac}]|_{ac}^2$  at the pulsation  $\omega_{ac}$  for a bead on which a “white noise” radiation pressure is exerted (hence maintaining it close to thermal equilibrium but at an effective temperature  $T_{eff}$  higher than room temperature), we can extract the value of  $F_{ac}$  by taking the mean value of all realizations. This value can then be used to calibrate the response function  $\chi''[\omega]$  and compare it with the steady-state fluctuation PSD  $2|x[\omega]|^2$ .

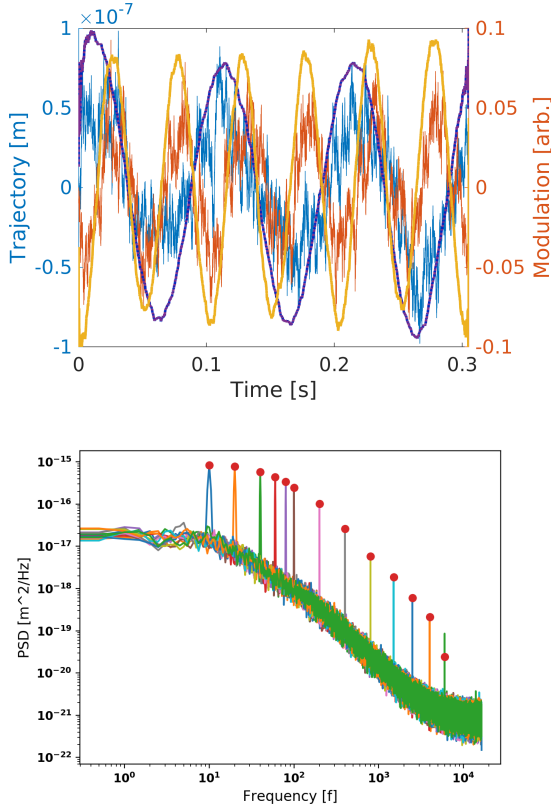


FIG. 13. (a) Active micro-rheological (AMR) experiment where the sinusoidal forcing of the system is monitored in the time domain. The recorded trajectories of the bead inside the trap are superimposed to the sinusoidal traces of the force for two different modulation frequencies. (b) Power spectral densities displayed together for different modulation frequencies of the external force drive. The Fourier components of each harmonic forcing are clearly seen as peaks in the PSD.

On Fig. 13 (a), we show the external drive in the time-domain and the motional response of the bead inside the trap for two different modulation frequencies. By repeating the procedure for frequencies ranging from 10 Hz to 6 kHz, the response of the bead is characterized over all the useful bandwidth (see Fig. 13 (b)). On Fig. 14, the values of  $\omega|x[\omega]|^2/2k_B T$  and  $\chi''[\omega]$  are plotted together for the probed

frequencies, for both the white noise and colored noise driven processes. We clearly observe that in both cases, the response functions associated with the mechanical susceptibilities fall back on the same trend. This trend is exactly the one associated with the white noise driven PSD as expected from Eq. (E5). In contrast, the spectral density of the colored noise driven process significantly departs from the FDT in Eq. (E5), and more particularly for the low frequencies of the active fluctuation spectrum. This is in agreement with other observations made recently in active systems [53], where the active mechanical processes mostly appear at low frequency, while the FDT is recovered for the thermally dominated high-frequency part.

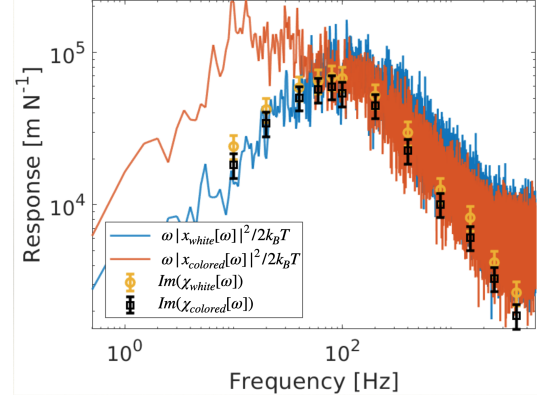


FIG. 14. We compare the measured values of  $\chi''[\omega]$  for white (open circles) and correlated (open squares) noise for different modulation frequencies  $\omega_{ac}$  and small sinusoidal perturbations with the stationary correlation spectra plotted as  $\omega|x[\omega]|^2/2k_B T$  for white (blue curve) and correlated (orange curve) noises. One immediately remarks the breaking of the FDT for the colored-noise driven process.

We note here that a simple observation of the breaking of the FDT can already be seen in our model described by Eq. (D1), where the fluctuating forces associated with the added noises  $\xi_t$  and  $\eta_t$  now possess an intrinsic correlation time due to the correlated nature of  $\eta_t$ , while the friction kernel  $\gamma$  is taken as instantaneous  $\Gamma(t, t') = \gamma\delta(t, t')$ . This choice has been shown to be valid in the experimental case [17], where the fluctuations of the active bath are not compensated by a dissipation with the same rate. In the limit of vanishing correlation times, the FDT is recovered as the noise is white ( $\delta$ -correlated) and its only effect is an effective change in temperature, as was already observed using a different experimental technique [55, 56].

## Appendix F: Thermodynamics

The application of stochastic thermodynamics to active matter has already been studied theoretically [9, 10, 13, 34, 35] and experimentally in some cases [15]. In this Appendix, we describe in detail how the stochastic heat can be efficiently used to describe and characterize the processes at play in our experiments. We first note that, in our experiments, our sys-

tem is brought to a Non-Equilibrium Steady-State (NESS) where the stationary stochastic laser drive maintains – through the action of radiation pressure – the system out of its equilibrium state at a given temperature and stiffness  $\kappa$ . Following the standard methods of stochastic energetics [40, 44], we write, from Eq. (D1), for our process

$$\left(\gamma\dot{x}_t - \gamma\sqrt{2D}\xi_t dt\right) dx = -\left(\kappa x_t + \gamma\sqrt{2D_a}\eta_t\right) dx. \quad (\text{F1})$$

The left-hand side is interpreted as the heat exchanged with the thermal bath  $\delta q = -\left(\gamma\dot{x} - \sqrt{2D}\xi_t dt\right) dx$ . Since the active force is stochastic, it produces no work. In fact, including a random force in the expression of work induces a violation of the Crooks relation [57]. The internal energy stays related to the potential energy  $dU = -\kappa x_t^2 dx$  and the remaining term  $\gamma\sqrt{2D_a}\eta_t dx$  is the energy exchanged with the active bath. Interpreted as a heat term [13], it can be evaluated from the right-hand side of Eq. (F1) as

$$\delta q(t) = \kappa \frac{dx^2}{dt} dt - \gamma\sqrt{2D_a}\eta_t \dot{x}_t dt, \quad (\text{F2})$$

which can be integrated to give the stochastic heat evaluation

$$q(t) = \int_0^t \kappa \frac{dx_s^2}{ds} ds - \gamma \int_0^t \sqrt{2D_a}\eta_s \dot{x}_s ds. \quad (\text{F3})$$

Finally, we compute the ensemble average heat, which will be expressed in terms of variance and cross-correlations

$$Q(t) \equiv \langle q(t) \rangle = \int_0^t \kappa \frac{d\langle x_s^2 \rangle}{ds} ds - \gamma \int_0^t \sqrt{2D_a} \langle \eta_s \dot{x}_s \rangle ds. \quad (\text{F4})$$

The first term is connected to the evolution of the variance. It vanishes in the steady-state and only accounts for the heat released during a transient evolution of the distribution. The second term can be computed analytically by injecting the differential equation Eq. (D1) for  $\dot{x}_t$ :  $\langle x_t \dot{\eta}_t \rangle = -\omega_0 \langle x_t \eta_t \rangle + \sqrt{2D_a}\alpha$ . The first term can be computed

$$\begin{aligned} \langle x_t \eta_t \rangle &= \int_0^t \sqrt{2D_a} \langle \eta_t \eta_s \rangle e^{-\omega_0(t-s)} ds \\ &= \alpha \int_0^t \sqrt{2D_a} e^{-\omega_c|t-s| - \omega_0(t-s)} ds \\ &= \frac{\sqrt{2D_a}\alpha}{\omega_0 + \omega_c} \left(1 - e^{-t(\omega_0 + \omega_c)}\right), \end{aligned} \quad (\text{F5})$$

and the second term

$$\begin{aligned} & -\gamma \int_0^t \sqrt{2D_a} \langle x_s \dot{\eta}_s \rangle ds \\ &= -\gamma \int_0^t \sqrt{2D_a} \left(-\omega_0 \langle x_s \eta_s \rangle + \sqrt{2D_a}\alpha\right) ds \\ &= 2\gamma D_a \alpha \left( \int_0^t \frac{\omega_0}{\omega_0 + \omega_c} \left[1 - e^{-s(\omega_0 + \omega_c)}\right] ds - t \right) \\ &= 2\gamma D_a \alpha \left( \frac{\omega_0}{\omega_0 + \omega_c} - 1 \right) t + \frac{2\gamma D_a \omega_0}{(\omega_0 + \omega_c)^2} (1 - e^{-t(\omega_0 + \omega_c)}), \end{aligned} \quad (\text{F6})$$

to give, after an exponential decorrelation at short times (just after the noise is turned on, a short-time regime that is never probed in our experiments), a linear heat expenditure with negative (since  $\omega_0 > 0$ ) slope  $2\gamma D_a \alpha \left(\frac{\omega_0}{\omega_0 + \omega_c} - 1\right)$  that account for the heat needed to maintain the system in its NESS. We note again that, in the white noise limit on an infinite bandwidth,  $\omega_c \rightarrow \infty$  makes this quantity vanish.

Therefore, if we discard the decorrelation after the noise is turned on, we obtain the following expression for the cumulative heat:

$$\begin{aligned} Q(t) &= \int_0^t \kappa \frac{d\langle x_s^2 \rangle}{ds} ds + 2\gamma D_a \alpha \left( \frac{\omega_0}{\omega_0 + \omega_c} - 1 \right) t \\ &\equiv Q_{EX}(t) + Q_{HK}(t), \end{aligned} \quad (\text{F7})$$

where the two quantities are reminiscent of the *excess* (EX) and *housekeeping* (HK) heat terms [45].

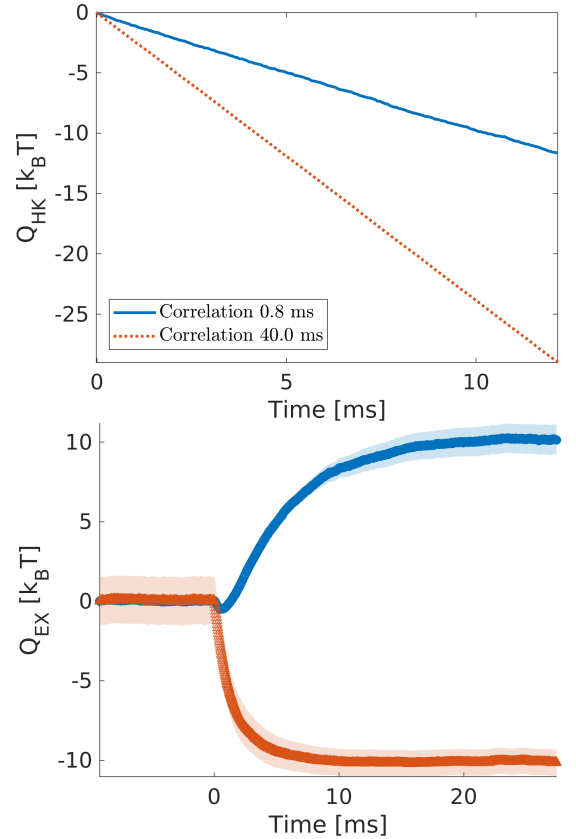


FIG. 15. (a) Measured heat necessary to keep the system in a NESS (in units of  $k_B T$ ) both for  $\tau_c = 0.8$  ms (blue line, before the STEP) and for  $\tau_c = 40$  ms (red dotted line, after the STEP). (b) Released heat measured through the transient both for a increasing correlation time (blue circles) and equivalently for a decreasing correlation time (red triangles).

In Fig. 15, we display the time evolution of these two quantities for the  $\tau_c(t)$  STEP protocol described above. Figure 15 (a) shows the heat necessary to maintain the NESS both before and after the change of  $\tau_c$ . As we see, changing the correlation

time changes the rate of heat dissipation. In Fig. 15 (b), the time-evolution of the excess heat discarded through the transient is plotted for both increasing or decreasing STEP of  $\tau_c$ . It is remarkable to stress that the quantity of heat  $\approx 10k_B T$  exchanged is the same for both cases.

Note that an alternative expression for the heat can be found in the context of active matter and active Ornstein-Uhlenbeck processes. These different approaches lead all to similar results, since Sekimoto's definition of heat as

$$\delta q = - \left( \gamma \dot{x} - \gamma \sqrt{2D} \xi_t dt \right) dx \quad (\text{F8})$$

is uniquely defined [6, 40]. The differences stem from the way to evaluate this quantity. In the description of non-reciprocal systems [58], the steady-state heat is computed as a sum of correlation between variables and velocities. In our case of unidirectional coupling, this simplifies to a term  $\sim \langle \eta_t \dot{x}_t \rangle$  which is the term we also obtain. Another definition is based on the deviation from the fluctuation dissipation relation, the Harada-Sasa relation [59] used in [6, 35], which, similarly to our calculations, gives a linear heat production in the steady state.

### Appendix G: Spectral entropy

The information content of the injected noise is measured by the spectral entropy  $H_s$  [20], which is precisely the Shannon entropy measured in the frequency domain. To evaluate this quantity and its relation to heat, we perform a series of measurement varying the correlation time of the noise  $\tau_c$  while keeping the other parameters constant, and test the robustness of the result for different sets of parameter (stiffness and noise intensity). For each experiment, an equivalent white noise experiment is also performed, that allows us to extract an effective temperature evaluated through equipartition:  $T_{eff} = \kappa \langle x^2 \rangle / k_B$ . We then compare  $Q_{EX} / k_B T_{eff}$  to  $H_s$ . The evaluation of  $H_s$  is done on the normalized power spectral density of the noise itself. In Fig. 16, we represent the normalized power spectral densities (PSD) for white and colored noises generated at 20 kHz, along with the spectral

boundaries used to get rid of the nonphysical part of the signal (high frequency noise of the electronics).

On this PSD, the spectral entropy is then evaluated as:

$$H_s = -k_B \sum_{i=1}^N P(\omega_i) \ln P(\omega_i), \quad (\text{G1})$$

where  $P(\omega_i) = S_\eta[\omega_i] / \sum_i S_\eta[\omega_i]$ , and  $S_\eta[\omega_i] = 2|\eta[\omega_i]|^2$  denotes the PSD of the signal  $\eta[\omega]$  at frequency  $\omega_i$ .

In the main text, we present the data from three different experiments. The first one is set with  $\kappa = 33.2$  pN/ $\mu\text{m}$  and a pushing laser maximal power of 150 mW, leading to a white noise effective temperature of 764.4 K. The second experiment is performed with  $\kappa = 14.8$  pN/ $\mu\text{m}$ , pushing laser power 19 mW, leading to  $T_{eff} = 531.8$  K. The third experiment is done with  $\kappa = 21.4$  pN/ $\mu\text{m}$ , pushing laser power

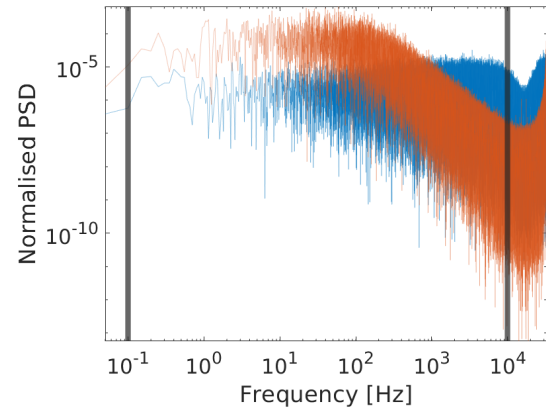


FIG. 16. Spectra of the white noise (blue line) and colored noise (orange line). The vertical black lines are the limits imposed on the calculation of the spectral entropy at 0.1Hz and  $10^4$ Hz.

40 mW, leading to  $T_{eff} = 943.6$  K. The strong influence of both the stiffness and noise intensity on effective temperature is clear. This influence however does not break the central relation shown in the main text between  $Q_{EX}$  and  $H_s$ .

- 
- [1] R. Rao and M. Esposito, Nonequilibrium thermodynamics of chemical reaction networks: Wisdom from stochastic thermodynamics, *Phys. Rev. X* **6**, 041064 (2016).
  - [2] X. Fang, K. Kruse, T. Lu, and J. Wang, Nonequilibrium physics in biology, *Rev. Mod. Phys.* **91**, 045004 (2019).
  - [3] P. Davies, Does new physics lurk inside living matter?, *Physics Today* **73**, 34 (2020).
  - [4] C. Bustamante, J. Liphardt, and F. Ritort, The nonequilibrium thermodynamics of small systems, *Phys. Today* **58**, 43 (2005).
  - [5] S. Ciliberto, Experiments in stochastic thermodynamics: Short history and perspectives, *Phys. Rev. X* **7**, 021051 (2017).
  - [6] J. T. Park, G. Paneru, C. Kwon, S. Granick, and H. K. Pak, Rapid-prototyping a Brownian particle in an active bath, *Soft Matter* **16**, 8122 (2020).
  - [7] G. Paneru, J. T. Park, and H. K. Pak, Transport and diffusion enhancement in experimentally realized non-gaussian correlated ratchets, *J. Phys. Chem. Lett.* **12**, 11078 (2021).
  - [8] A. Militaru, M. Innerbichler, M. Frimmer, F. Tebbenjohanns, L. Novotny, and C. Dellago, Escape dynamics of active particles in multistable potentials, *Nature Communications* **12**, 2446 (2021).
  - [9] T. Speck, Stochastic thermodynamics for active matter, *EPL (Europhysics Letters)* **114**, 30006 (2016).
  - [10] U. M. B. Marconi, A. Puglisi, and C. Maggi, Heat, temperature and clausius inequality in a model for active brownian particles, *Sci. Rep.* **7**, 46496 (2017).
  - [11] C. Sandford, A. Y. Grosberg, and J.-F. Joanny, Pressure and flow of exponentially self-correlated active particles, *Phys. Rev.*

- E 96, 052605 (2017).**
- [12] D. Martin, J. O’Byrne, M. E. Cates, E. Fodor, C. Nardini, J. Tailleur, and F. van Wijland, Statistical mechanics of active Ornstein-Uhlenbeck particles, *Phys. Rev. E* **103**, 032607 (2021).
- [13] L. Dabelow, S. Bo, and R. Eichhorn, Irreversibility in active matter systems: Fluctuation theorem and mutual information, *Phys. Rev. X* **9**, 021009 (2019).
- [14] T. Speck, Modeling of biomolecular machines in non-equilibrium steady states (2021), [arXiv:2109.03516](https://arxiv.org/abs/2109.03516) [[cond-mat.stat-mech](https://arxiv.org/archive/cond-mat)].
- [15] A. Argun, A.-R. Moradi, E. Pinçe, G. B. Bağcı, A. Imparato, and G. Volpe, Non-boltzmann stationary distributions and nonequilibrium relations in active baths, *Phys. Rev. E* **94**, 062150 (2016).
- [16] C. Maggi, M. Paoluzzi, N. Pellicciotta, A. Lepore, L. Angelani, and R. Di Leonardo, Generalized energy equipartition in harmonic oscillators driven by active baths, *Phys. Rev. Lett.* **113**, 238303 (2014).
- [17] C. Maggi, M. Paoluzzi, L. Angelani, and R. Di Leonardo, Memory-less response and violation of the fluctuation-dissipation theorem in colloids suspended in an active bath, *Scientific Reports* **7**, 17588 (2017).
- [18] S. Hurst, B. E. Vos, M. Brandt, and T. Betz, Intracellular softening and increased viscoelastic fluidity during division, *Nature Physics* **17**, 1270 (2021).
- [19] A. V. Taubenberger, B. Baum, and H. K. Matthews, The mechanics of mitotic cell rounding, *Frontiers in Cell and Developmental Biology* **8**, 687 (2020).
- [20] N. Zaccarelli, B.-L. Li, I. Petrosillo, and G. Zurlini, Order and disorder in ecological time-series: Introducing normalized spectral entropy, *Ecological Indicators* **28**, 22 (2013), 10 years Ecological Indicators.
- [21] R. Astumian and I. Deényi, Fluctuation driven transport and models of molecular motors and pumps, *Eur. Biophys. J.* **27**, 474 (1998).
- [22] Y. Ezber, V. Belyy, S. Can, and A. Yildiz, Dynein harnesses active fluctuations of microtubules for faster movement, *Nat. Phys.* **16**, 312 (2020).
- [23] H. Linke, B. Höcker, K. Furuta, N. R. Forde, and P. M. Curmi, Synthetic biology approaches to dissecting linear motor protein function: towards the design and synthesis of artificial autonomous protein walkers, *Biophys. Rev.* **12**, 1041 (2020).
- [24] G. Szamel, Self-propelled particle in an external potential: Existence of an effective temperature, *Phys. Rev. E* **90**, 012111 (2014).
- [25] E. Fodor, C. Nardini, M. E. Cates, J. Tailleur, P. Visco, and F. van Wijland, How far from equilibrium is active matter?, *Phys. Rev. Lett.* **117**, 038103 (2016).
- [26] C. Bechinger, R. Di Leonardo, H. Löwen, C. Reichhardt, G. Volpe, and G. Volpe, Active particles in complex and crowded environments, *Rev. Mod. Phys.* **88**, 045006 (2016).
- [27] P. Jung and P. Hänggi, Dynamical systems: A unified colored-noise approximation, *Phys. Rev. A* **35**, 4464 (1987).
- [28] M. S. Miguel and J. M. Sancho, A colored-noise approach to Brownian motion in position space. corrections to the smolucski equation, *Journal of Statistical Physics* **22**, 605 (1980).
- [29] We stress that the amplitude coefficient  $\alpha$  for the colored noise  $\eta_t$  is fixed digitally: its impact on the motional dynamics described below by Eq. (D1) is taken over by the active diffusivity  $D_a$ . However, as clear from in Eq. (B1), it has a fixed dimension (Hz) and thus will appear in the evaluation of the MSD.
- [30] X.-L. Wu and A. Libchaber, Particle diffusion in a quasi-two-dimensional bacterial bath, *Phys. Rev. Lett.* **84**, 3017 (2000).
- [31] C. Sandford and A. Y. Grosberg, Memory effects in active particles with exponentially correlated propulsion, *Phys. Rev. E* **97**, 012602 (2018).
- [32] R. Metzler and J. Klafter, The random walk’s guide to anomalous diffusion: a fractional dynamics approach, *Physics Reports* **339**, 1 (2000).
- [33] N. M. Mutothya, Y. Xu, Y. Li, and R. Metzler, Characterising stochastic motion in heterogeneous media driven by coloured non-Gaussian noise, *Journal of Physics A: Mathematical and Theoretical* (2021).
- [34] S. Chaki and R. Chakrabarti, Entropy production and work fluctuation relations for a single particle in active bath, *Physica A: Statistical Mechanics and its Applications* **511**, 302 (2018).
- [35] S. Chaki and R. Chakrabarti, Effects of active fluctuations on energetics of a colloidal particle: Superdiffusion, dissipation and entropy production, *Physica A: Statistical Mechanics and its Applications* **530**, 121574 (2019).
- [36] The diffusion of free-like Brownian motion measured in the short-time  $\tau \ll \gamma/\kappa$  limit of the MSD is driven by the same temperature as the long-time of the MSD where the motional dynamics is dominated by the trapping process, and by the same temperature fixing, through equipartition the motional variance  $\langle x_t^2 \rangle$  [39].
- [37] J. Łuczka, Non-markovian stochastic processes: Colored noise, *Chaos* **15**, 026107 (2005).
- [38] E. Dieterich, J. Camunas-Soler, M. Ribezzi-Crivellari, U. Seifert, and F. Ritort, Single-molecule measurement of the effective temperature in non-equilibrium steady states, *Nature Physics* **11**, 971 (2015).
- [39] R. Goerlich, M. Li, S. Albert, G. Manfredi, P.-A. Hervieux, and C. Genet, Noise and ergodic properties of brownian motion in an optical tweezer: Looking at regime crossovers in an ornstein-uhlenbeck process, *Phys. Rev. E* **103**, 032132 (2021).
- [40] K. Sekimoto, Langevin Equation and Thermodynamics, *Progress of Theoretical Physics Supplement* **130**, 17 (1998), <https://academic.oup.com/ptps/article-pdf/doi/10.1143/PTPS.130.17/5213518/130-17.pdf>.
- [41] I. A. Martínez, E. Roldán, L. Dinis, D. Petrov, and R. A. Rica, Adiabatic processes realized with a trapped Brownian particle, *Phys. Rev. Lett.* **114**, 120601 (2015).
- [42] I. A. Martinez, E. Roldán, L. Dinis, and R. Rica, Colloidal heat engines: a review, *Soft Matter* **13**, 22 (2017).
- [43] J. A. Albay, Z.-Y. Zhou, C.-H. Chang, and Y. Jun, Shift a laser beam back and forth to exchange heat and work in thermodynamics, *Sci. Rep.* **11**, 1 (2021).
- [44] K. Sekimoto, *Stochastic energetics* (Springer-Verlag, Berlin Heidelberg, 2010).
- [45] U. Seifert, Stochastic thermodynamics, fluctuation theorems and molecular machines, *Reports on Progress in Physics* **75**, 126001 (2012).
- [46] G. Woehlke and M. Schliwa, Walking on two heads: the many talents of kinesin, *Nature Reviews Molecular Cell Biology* **1**, 50 (2000).
- [47] T. Ariga, M. Tomishige, and D. Mizuno, Nonequilibrium energetics of molecular motor kinesin, *Phys. Rev. Lett.* **121**, 218101 (2018).
- [48] T. Ariga, K. Tateishi, M. Tomishige, and D. Mizuno, Noise-induced acceleration of single molecule kinesin-1, *Phys. Rev. Lett.* **127**, 178101 (2021).
- [49] R. Landauer, Irreversibility and heat generation in the computing process, *IBM Journal of Research and Development* **5**, 183 (1961).
- [50] M. P. Frank, Physical foundations of Landauer’s principle, [ArXiv 10.1007/978-3-319-99498-7](https://arxiv.org/abs/10.1007/978-3-319-99498-7) (2018).

- [51] M. B. Plenio and V. Vitelli, The physics of forgetting: Landauer's erasure principle and information theory, *Contemp. Phys.* **42**, 25 (2001).
- [52] E. Lutz and S. Ciliberto, Information: From maxwell's demon to landauer's eraser, *Phys. Today* **68**, 30 (2015).
- [53] H. Turlier, D. A. Fedosov, B. Audoly, T. Auth, N. S. Gov, C. Sykes, J.-F. Joanny, G. Gompper, and T. Betz, Equilibrium physics breakdown reveals the active nature of red blood cell flickering, *Nature Physics* **12**, 513 (2016).
- [54] G. Schnoering, Y. Rosales-Cabara, H. Wendehenne, A. Canaguier-Durand, and C. Genet, Thermally limited force microscopy on optically trapped single metallic nanoparticles, *Phys. Rev. Applied* **11**, 034023 (2019).
- [55] I. A. Martínez, E. Roldán, J. M. R. Parrondo, and D. Petrov, Effective heating to several thousand kelvins of an optically trapped sphere in a liquid, *Phys. Rev. E* **87**, 032159 (2013).
- [56] P. Mestres, I. A. Martínez, A. Ortiz-Ambriz, R. A. Rica, and E. Roldan, Realization of nonequilibrium thermodynamic processes using external colored noise, *Phys. Rev. E* **90**, 032116 (2014).
- [57] J. R. Gomez-Solano, L. Bellon, A. Petrosyan, and S. Ciliberto, Steady-state fluctuation relations for systems driven by an external random force, *EPL (Europhysics Letters)* **89**, 60003 (2010).
- [58] S. A. M. Loos and S. H. L. Klapp, Irreversibility, heat and information flows induced by non-reciprocal interactions, *New Journal of Physics* **22**, 123051 (2020).
- [59] T. Harada and S.-I. Sasa, Equality connecting energy dissipation with a violation of the fluctuation-response relation, *Phys. Rev. Lett.* **95**, 130602 (2005).